Evidence of nuclear quadrupole interaction in $BaTi_{0.7}Sn_{0.3}O_3$ relaxor around dielectric maxima: A synchrotron-based ^{119}Sn hyperfine interaction study

Meenal Dhanetwal [1], Akash Surampalli [2], Sven Velten [3], Deepak Prajapat [3], Anjali Panchwanee [3], Sourav Mukherjee [1], Chandana Mondal [1], Ganesh Bera [1,4], Ilya Sergeev [3] and V. Raghavendra Reddy [1,*]

[1] *UGC-DAE Consortium for Scientific Research, University Campus, Khandwa Road, Indore 452001, India*

[2] *Department of Materials Science and Engineering, University of California, Berkeley, Berkeley, California 94720, USA*

[3] *Deutsches Elektronen-Synchrotron - A Research Centre of the Helmholtz Association, 22607 Hamburg, Germany*

[4] *Applied Physics Department, Institute of Materials Science (ICMUV), Universidad de Valencia, 46100, Burjassot, Valencia, Spain*

(Received 10 April 2024; revised 25 June 2024; accepted 29 July 2024; published 19 August 2024)

The present work reports the ferroelectric (FE) element/site specific spectroscopic measurements in $BaTi_{0.7}$ $^{119}Sn_{0.3}$ O_3 relaxor using ^{119}Sn hyperfine interaction studies. The relaxor properties in the studied sample are confirmed from the macroscopic measurements such as temperature dependent dielectric constant measurements. The presence of quadrupole splitting (QS) below its dielectric maxima (T_m) is confirmed unambiguously using synchrotron radiation perturbed angular correlation experiments. Further, temperature dependent nuclear forward scattering data clearly depict the development of QS below T_m. Finite values of QS with temperature, below T_m, unambiguously indicate the development of electric field gradient around Sn/Ti sites in $BaTi_{0.7}$ $^{119}Sn_{0.3}$ O_3 relaxor, emphasizing the applicability of conventional FE models in explaining relaxor properties. The phonon density of states (PDOS) obtained from nuclear inelastic scattering measurements has been found to qualitatively match the results of PDOS calculated from molecular dynamics simulations and experimental Raman modes that are considered to be characteristic of Ti site in $BaTiO_3$.

DOI: 10.1103/PhysRevB.110.054205

I. INTRODUCTION

Relaxors have gained popularity in recent years due to their unusual polarization behavior and functional characteristics [1]. Lead-free relaxors, such as those based on barium titanate, $BaTiO_3$ (BTO), have received a lot of attention due to their nontoxic nature, high dielectric permittivity, several phase transitions, possibility of tuning transition temperature close to room temperature and broad frequency dispersive permittivity peak vs temperature as compared to other such systems [2,3]. It was suggested that the existence of polar nanoregions (PNRs) are responsible for frequency dispersion of dielectric constant values in relaxors.

Unlike traditional lead-based relaxors, which exhibit nominal charge disorder (as in $PbMg_{1/3}Nb_{2/3}O_3$), doped BTO materials exhibit relaxor behavior even in the absence of the charge disorder, making them an intriguing research area [4,5]. Earlier relaxor phenomenological models were concerned with explaining the dielectric, polarization behavior with electric-field/temperature. However, they lack an explanation for the observed soft mode behavior, fano resonance, and structural changes in relaxors [4,5]. Recently developed first-principles models of these relaxor materials successfully demonstrate both structural and relaxation phenomena in relaxors, simulating a wide range of relaxor features [6].

In our recent studies on 30% Sn substituted $BaTiO_3$($BaTi_{0.7}Sn_{0.3}O_3$), we have demonstrated the relaxor behavior from dielectric and polarization data revealing dispersion in dielectric constant, slim hysteresis loops and remnant polarization well above the dielectric temperature maximum (T_m). Further, we have demonstrated that the system undergoes structural modifications associated with changes in polarization in a wide temperature range in $BaTi_{0.7}Sn_{0.3}O_3$ [4]. Combining complimentary experimental methods such as x-ray diffraction (XRD), Raman spectroscopy, x-ray absorption spectroscopy, and ^{119}Sn Mössbauer spectroscopy we were able to coherently identify local structural counterparts associated with the relaxor properties in $BaTi_{0.7}Sn_{0.3}O_3$, hence drawing a connection with the dipole dynamics and providing inputs for a deeper understanding beyond the phenomenological models [7,8].

It may be noted that in displacivelike ferroelectric transitions, for example in the case of BTO, $PbTiO_3$ etc., loss of inversion symmetry is always associated with an onset of polarization. This results in changes for the interaction between nuclear quadrupole moment and electric field gradient (EFG) i.e., quadrupole splitting (QS) values. Therefore, the estimation of hyperfine parameters, especially QS was actively pursued by many groups in exploring the ferroelectric (FE) materials [9–14]. Theoretical studies establishing the direct relation between FE polarization, local distortion and EFG are reported in recent literature [15]. Experimental methods such as Mössbauer, perturbed angular correlations (PAC), nuclear magnetic resonance (NMR) etc., that can probe hyperfine interactions have been used in this direction. For example, temperature dependent PAC

*Contact author: varimalla@yahoo.com; vrreddy@csr.res.in

measurements have been employed to measure the EFG at (Ti,Zr) sites in $PbTi_{1-x}Zr_xO_3$ based ferroelectrics [13,14].

Either the variation of QS or the associated quantities such as V_{zz}, asymmetry parameter (η), quadrupole frequency (ω_q) etc., as a function of temperature are reported for the materials that exhibited robust FE ordering [9–14]. Such hyperfine studies are very limited in relaxors [4,16]. In our recent study on $BaTi_{0.7}Sn_{0.3}O_3$ relaxor, we did not observe obvious splitting of the Mössbauer absorption line due to the quadrupole interaction. However, the width of the line shows anomalous increase below T_m, that can be an indication of the EFG appearance [4]. It is worth mentioning here that the synchrotron based perturbed angular correlation (SRPAC) is a useful experimental method for the measurements of a small energy splitting of the hyperfine interactions. This advantage comes from the independence of the signal from the sample thickness and from the radioactive source line broadening. The capability of the SRPAC method for exploring hyperfine interactions, was demonstrated in several works [17–20]. In view of this, in the present work we have undertaken the SRPAC study to unambiguously prove the presence of QS below dielectric maxima in $BaTi_{0.7}Sn_{0.3}O_3$ relaxor. With this input, detailed temperature dependent nuclear forward scattering (NFS) measurements are also carried out to elucidate the quantitative variation of QS in $BaTi_{0.7}Sn_{0.3}O_3$ relaxor across its dielectric maxima. The observed variation of QS with temperature indicate the signatures of dynamic relaxation of PNRs.

Further, to probe the vibrational modes associated with Sn site, ^{119}Sn nuclear inelastic scattering (NIS) measurements are carried out at two temperatures covering T_m. Since NIS is sensitive to Mössbauer active element, the phonon density of states (PDOS) obtained from NIS measurements would be specific to ^{119}Sn nucleus unlike other measurements such as Raman spectroscopy, neutron inelastic scattering, inelastic x-ray scattering etc., which give the consolidated PDOS of the entire system [21]. The obtained PDOS from NIS measurements is compared with molecular dynamics simulations and the experimental Raman modes that are considered to be characteristic of the Ti site in BTO.

II. EXPERIMENTAL

Polycrystalline 30% Sn substituted BTO ($BaTi_{0.7}Sn_{0.3}O_3$) is prepared with conventional solid-state sintering method starting from high purity ($\geqslant$ 99.9%) oxide and carbonate precursors. Unlike the previous case [4], ^{119}Sn enriched SnO_2 is used as precursor in the present study so as to do the ^{119}Sn nuclear resonance experiments. X-ray diffraction (XRD) measurements are carried out using laboratory based system with 0.154 nm radiation. Dielectric measurements were performed using precision LCR meter E4980 and in-house developed sample holder with 1 V ac signal at different frequencies in the temperature range 100-300 K, while cooling the sample. Room temperature ^{119}Sn Mössbauer measurements were carried out in transmission mode using a standard PC-based Mössbauer spectrometer equipped with a WissEl velocity drive in constant acceleration mode. The spectrometer was calibrated with natural iron at room temperature and the reported isomer shift values are with respect to SnO_2. Low temperature ^{119}Sn NFS, NIS, and SRPAC measurements are performed at beamline P01, PETRA III, DESY, Hamburg. NFS data is analyzed with Nuclear Elastic X-ray scattering Universal Software (NEXUS) program [22]. The SRPAC spectrum was measured at 15 K in vertical and horizontal geometries perpendicular to the beam path similar to the setup described by Dimitrios Bessas *et al.* [20]. The detector and the cryostat were rotated together while changing the experimental geometry [20].

III. NUMERICAL MODEL AND DETAILS OF SIMULATIONS

In the present work, molecular dynamics (MD) simulations of a model $BaTi_{0.7}Sn_{0.3}O_3$ system are carried out using an open source classical MD simulation code LAMMPS [23]. In the MD simulations, it is considered that particles interact with a pairwise potential consisting three parts viz., (i) repulsive contribution C/r^{12}, (ii) short-range Morse function with a cutoff distance of 15Å, and (iii) long-range Coulomb potential, with the following form:

$$V(r) = \frac{q_i q_j}{r} + D_{ij}[\{1 - e^{-a_{ij}(r-r_0)}\}^2 - 1] + \frac{C_{ij}}{r^{12}}. \quad (1)$$

The repulsive contribution is necessary to prevent overlap between atoms. The long-range Coulomb interactions are calculated by using the Ewald summation [24]. Detailed discussion on the interaction potential and parameters can be found in Ref. [25]. The values of the parameters D_{ij}, a_{ij}, r_0 are shown in Table-I:

We use a rigid-ionic model with partial charges to account for the partial covalency of BTO. Following the success of Beest-Kramer-Santen (BKS) [26] model, partial charge models have been extensively used in the recent years for more accurate results for structural as well as mechanical properties. As in the BKS model, charge on the oxygen atoms are kept fixed at $-1.2e$. To maintain the self- consistency of the force field, the partial charges on the cations are assigned accordingly. Ba atoms have charge $1.2e$ and Ti/Sn atoms have charge $2.4e$. It should be noted that these values should be considered only as parameters of the model [25] and should not be compared with the actual charges of individual atoms.

The simulations were started with a super-cell consisting of $10 \times 10 \times 10$ unit cells of $BaTiO_3$ in three dimensions. After that 30% of Ti atoms are chosen randomly and replaced by Sn atoms. The box-length considered is 4.04 nm and periodic boundary conditions are applied in all three directions. Initially random velocities are assigned to the particles from

TABLE I. Ba-O, Ti-O, Sn-O, and O-O interatomic potential parameters. The cutoff distance for the short-range interactions is set to 15 Å.

Element	D_{ij} (eV)	a_{ij} (Å^{-2})	r_0 (Å)	C_{ij} (eVÅ^{12})
$Ba^{1.2}$-$O^{-1.2}$	0.065011	1.547596	3.393410	5.0
$Ti^{2.4}$-$O^{-1.2}$	0.024235	2.254703	2.708943	1.0
$Sn^{2.4}$-$O^{-1.2}$	0.079400	2.156770	2.633076	3.0
$O^{-1.2}$-$O^{-1.2}$	0.042395	1.379316	3.618701	22.0

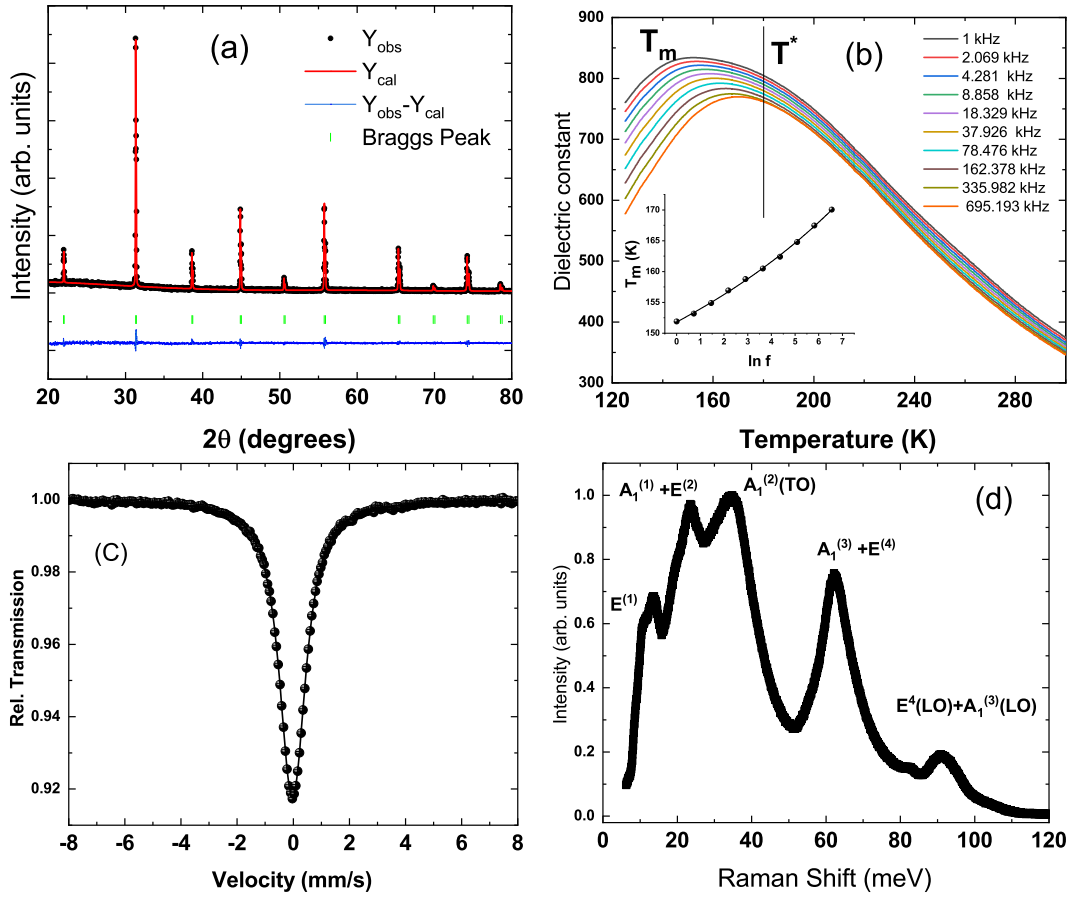

FIG. 1. Basic characterization of $BaTi_{0.7}\,^{119}Sn_{0.3}\,O_3$. (a) Room temperature x-ray diffraction (XRD) pattern. The experimental XRD data is profile fitted with FullProf program. (b) Temperature dependent dielectric constant and the inset of (b) show the Vogel-Fulcher fit to the variation of T_m as a function of frequency as discussed in the text. (c) Room temperature ^{119}Sn Mössbauer data, symbols in (c) indicate the data points and the solid line is the best fit to the data. (d) Room temperature Raman data with the indicated vibrational modes.

a Maxwell-Boltzmann distribution at temperature T=296 K. After generating the sample we minimize its energy with conjugate gradient method until force on each atom vanished. We then (i) heat the sample up to 1300 K in 1 nanosecond (ns), (ii) thermalize the sample at 1300 K for 1 ns, (iii) reduce the temperature of the sample to low temperature (either 40 K or 296 K) in 1 ns. During the above four steps we keep the number of particles (N), and volume (V) fixed. Finally we perform a pressure minimization—cell relaxation—for 1 ns. Noose-Hoover thermostat with relaxation time 0.1 ps and barostat with relaxation time 1.0 ps [27–30] are used to maintain constant temperature and pressure, respectively.

IV. RESULTS

A. XRD, Dielectric, Mössbauer and Raman measurements

In order to ensure that the prepared ^{119}Sn enriched $BaTi_{0.7}Sn_{0.3}O_3$ sample properties are same as that of our earlier $BaTi_{0.7}Sn_{0.3}O_3$, which was prepared with natural SnO_2, the basic characterization such as XRD, temperature dependent dielectric constant data, ^{119}Sn Mössbauer and Raman spectroscopy measurements are carried out in the present work. The full profile fitting analysis of XRD pattern has been carried out using FULLPROF program [31] and the refinement reveals a cubic structure (space group 221) in the present work as shown in Fig. 1(a). The dielectric data of the present work, as shown in Fig. 1(b) agree very well with our earlier work and literature [4,32,33]. The dielectric maximum temperature (T_m) is found to shift towards higher temperature with increasing frequency which is a characteristic of relaxor ferroelectrics [1]. Further, the variation of T_m with frequency and the fitting using Vogel-Fulcher (VF) formalism defined as,

$$\tau = \tau_0 \exp\left[\frac{E}{k_B(T_m - T_f)}\right], \tag{2}$$

as shown in the inset of Fig. 1(b) confirms the relaxor behavior. Temperature T^* is identified at 180 K from the dielectric data as explained in our earlier work [4]. Room temperature ^{119}Sn Mössbauer data [Fig. 1(c)] indicate an almost zero center shift indicating a Sn^{4+} oxidation state, i.e., isovalent substitution and the obtained width (Γ) of Mössbauer data is 1.03 ± 0.02 mm/s. Room temperature Raman data is also observed to agree with literature and the mode assignment is carried out by comparing the literature [34–38], as shown in Fig. 1(d). Summarizing this, the prepared ^{119}Sn enriched $BaTi_{0.7}\,^{119}Sn_{0.3}\,O_3$ sample properties are same as that of our earlier results on sample $BaTi_{0.7}Sn_{0.3}O_3$ [4].

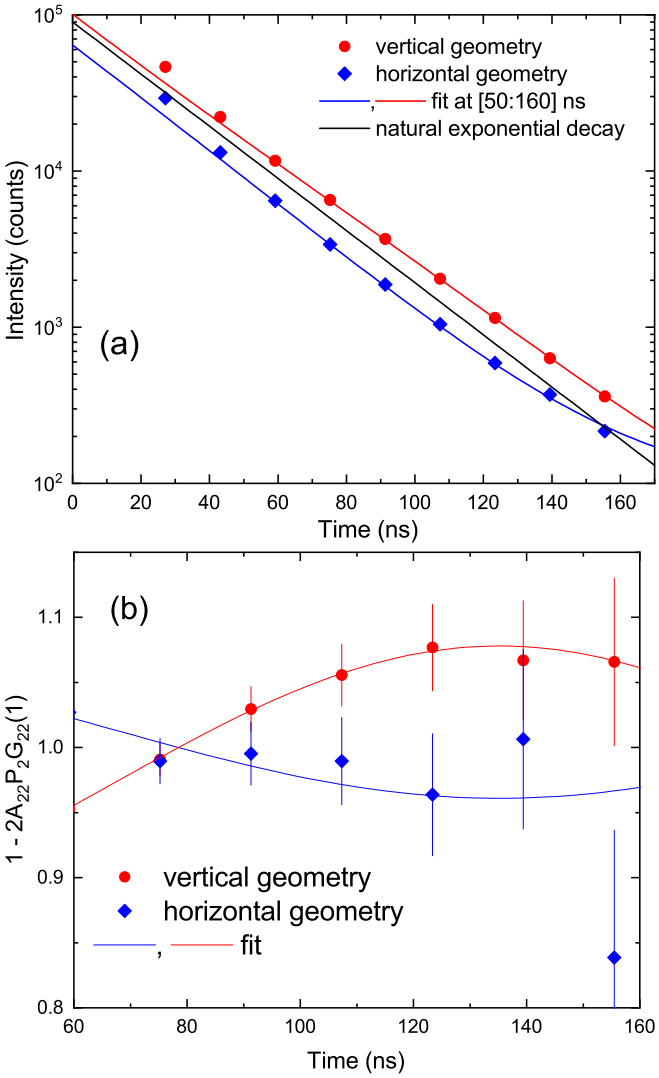

FIG. 2. Synchrotron radiation perturbed angular correlation (SRPAC) data of $BaTi_{0.7}{}^{119}Sn_{0.3}O_3$. (a) Time dependence of the incoherent scattering intensity measured in the vertical and horizontal geometries at 15 K. (b) Time dependence of the anisotropy, measured in the vertical (red) and horizontal(blue) geometries at 15K. The lines shows fit by the model as discussed in the text.

B. Synchrotron Radiation Perturbed Angular Correlation (SRPAC) measurements

Figure 2(a) shows the time dependence of the observed SRPAC signal in different geometries and the simulation of the natural decay. The pure SRPAC signal for the highly linearly $\sigma-$ polarized synchrotron radiation is described by

$$I(t) = I_0 \exp\left(\frac{-t}{\tau}\right)[1 - 2P_2A_{22}G_{22}(t)] + b, \qquad (3)$$

where I_0 is the intensity scaling factor, A_{22} is the anisotropy factor, which is determined by the both nuclear transition and details of the experimental arrangement, P_2 is a scattering geometry factor, i.e., $P_2 = 1$ for the vertical geometry, $P_2 = -1/2$ for the horizontal geometry. $G_{22}(t)$, the perturbation factor which describes the time modulation of the signal due to hyperfine interactions (considering only an isotropic electric quadrupole hyperfine interaction) is given by

$$G_{22}(t) = \left(1 + 4\cos\frac{\hbar c}{E_\gamma}\Omega t\right)/5, \qquad (4)$$

where Ω is the QS value. The measured data deviates from the pure SRPAC signal due to the contribution of the nontrivial multiple scattering phenomena and radiation trapping effects present due to the high Lamb-Mössbauer factor [17–20]. The first contribution appears at the early times (below 50 ns), which will be excluded from the fit. The second effect will be accounted for by taking τ, which is supposed to be the natural decay rate, as a fitted parameter. The fit of the SRPAC data in two geometries was performed simultaneously with the common fitting parameters τ, A_{22}, and Ω, and one parameter I_0 for each geometry. The background b was taken according to the measurements time and known detector noise rate. The obtained results of SRPAC data analysis are further discussed in Sec. V.

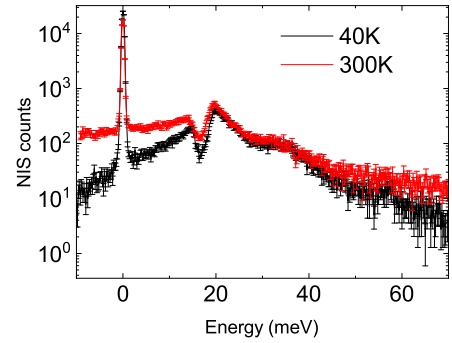

FIG. 3. ^{119}Sn nuclear inelastic scattering data of $BaTi_{0.7}{}^{119}Sn_{0.3}O_3$ at 40K (black color) and 300K (red color). The obtained phonon density of states (PDOS) are shown in Fig. 7.

C. ^{119}Sn Nuclear inelastic scattering (NIS) measurements

Figure 3 shows the obtained NIS spectra of the sample at two temperatures, one at room temperature and another one below T_m at 40 K as obtained from the analysis of the detailed thermal balance of the negative and positive parts of the spectrum. The NIS spectra consist of elastic line of nuclear incoherent scattering (centered around zero energy) and the multiphonon contribution to the nuclear inelastic absorption [21], with the peaks at higher energy as shown in Fig. 3. The extracted parameters from the analysis of NIS data are shown in Table II.

TABLE II. Parameters extracted from the analysis of NIS data as shown in Fig. 3. T is the temperature, A is the area under PDOS (should be 1), f_{LM} is the Lamb-Mössbauer factor, U is the internal energy per atom, F is the mean force constant per atom, S_{vib} is vibrational energy per atom & k_B is the Boltzmann constant.

T (K)	A	f_{LM}	U (meV)	F (Nm^{-1})	S_{vib} (3 k_B)
296	0.999(1)	0.660(5)	8.5(4)	298(24)	1.75(2)
40(3)	1.002(1)	0.879(1)	37(1)	333(24)	0.06(1)

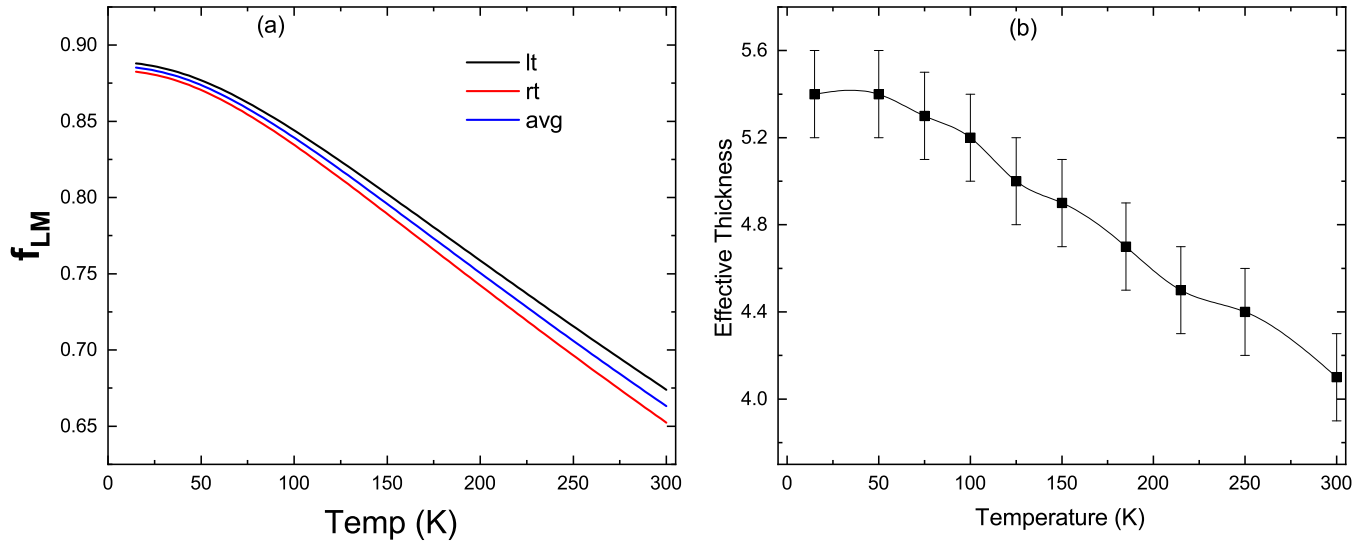

FIG. 4. (a) Extrapolated temperature variation of Lamb-Mössbauer parameter (f_{LM}) obtained from Eq. (5) considering the experimental values obtained from low temperature (lt) and room temperature (rt) NIS data. Average value (avg) of f_{LM}, which is considered for the analysis of NFS data is also shown. (b) Temperature variation of effective thickness of the sample.

The Lamb-Mössbauer parameter (f_{LM}) for the lowest and room temperature were directly measured via NIS. Based on the two-phonon density of states we had calculated the f_{LM} for different temperatures within the harmonic approximation given by the following equation and the results are shown in Fig. 4:

$$f_{LM} = \exp\left(-2E_R \int_0^\infty \frac{g(E)}{E}\left(\frac{1}{2} + \frac{1}{\exp(\beta E) - 1}\right) dE\right), \tag{5}$$

where E_R is recoil energy (2.54 meV for ^{119}Sn), g(E) is phonon density of state (PDOS), $\beta = 1/(k_B T)$, k_B is Boltzmann constant and T is temperature. For the analysis of the NFS data in the present work, we had used the average value of f_{LM}, also shown in Fig. 4. The obtained effective thickness values are calculated using the average f_{LM} and the thickness from the fit (70 μm), is also shown in the Fig. 4.

Perusal of Table II indicate that the force constant (F) is practically same for the temperatures below and above T_m, as expected. Usually for robust FE materials exhibiting first-order phase transition and associated mode-softening, the F value goes to zero below the transition temperatures. This is not the case in the present work and therefore the F values remain same as a function of temperature. But, as expected there is an increase in internal energy (U) and decrease of vibrational energy per atom (S_{vib}) at low temperatures, indicating the physical validity of the NIS data analysis. From the NIS data, the PDOS of ^{119}Sn is obtained (Fig. 7) and will be discussed in Sec. V.

D. Molecular Dynamics (MD) Simulations

After the standard thermalization procedure, as discussed in Sec. III, we get a box size $4.05 \times 4.05 \times 4.05$ nm^3 at 40K and $4.04 \times 4.04 \times 4.04$ nm^3 at 300K. The PDOS are calculated at 300 and 40 K corresponding to whole system, Sn/Ti, Ba, O- sites, and the results are shown in Fig. 5. It may be mentioned here that it is not possible, using our tool, to separate the contribution of Ti atoms from Sn atoms to the PDOS data.

The characteristic vibrational modes of BTO system in its different phases such as cubic (C), tetragonal (T), orthorhombic (O) and rhombhohedral (R) have been calculated in past by using first-principles calculations within the density functional theory (DFT) employing plane wave (PW) DFT, full-potential linearized augmented PW DFT, linear combination of atomic orbitals, etc. [36–40]. However, the MD simulations are limited in literature for the BTO based compounds, except the recent work on oxygen diffusion and flexoelectricity in BTO [41,42]. Nonetheless, the obtained vibrational density of states with MD simulations in the present work qualitatively agree with the reported DFT results [36–40]. Further, qualitatively the MD simulated PDOS at 300 and 40 K is same, consistent with the fact that there is no macroscopic change of symmetry in the studied relaxor across T_m.

E. ^{119}Sn Nuclear forward scattering (NFS) measurements

NFS measurements are carried out at different temperatures covering the region of dielectric maxima of $BaTi_{0.7}Sn_{0.3}O_3$ relaxor. Since the hyperfine splitting is expected to be small in such relaxors, the data fitting/analysis has to be ensured by adopting a consistent model. Parameters such as density, isotope abundance, thickness of the sample and its distribution (Gaussian) etc., were considered to be same for all temperatures. Whereas the f_{LM} values obtained from NIS data (Fig. 3) are employed in analyzing the NFS data. The NFS data was initially fitted assuming that the beating is only a dynamical feature for different temperatures. With this model the fitting was observed to be acceptable at high temperatures, however the quality of the fitting was not good for low temperatures, below (T_m). This indicated

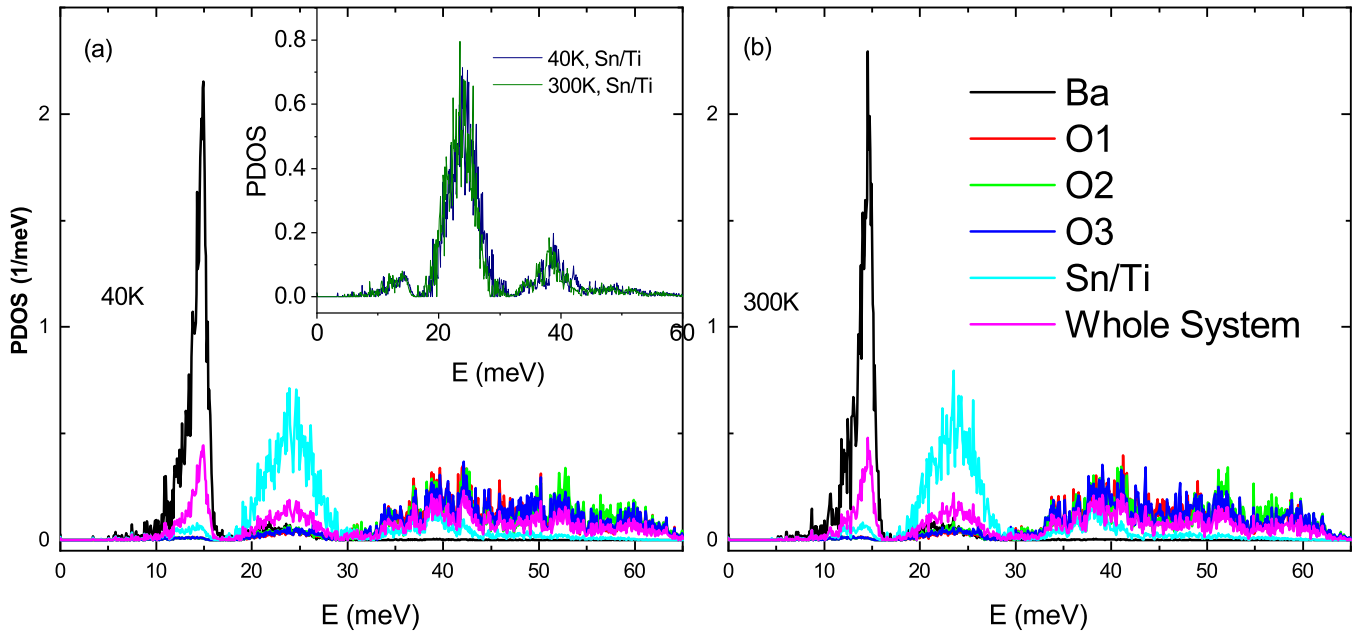

FIG. 5. The molecular dynamics (MD) simulation of phonon density of states (PDOS) for $BaTi_{0.7}Sn_{0.3}O_3$ corresponding to whole system, Ba atoms, three O atoms and Ti/Sn atoms at (a) 40 K (b) 300 K. Inset show the modes corresponding to Ti/Sn atoms at 300 and 40 K.

the development of hyperfine splitting at low temperatures, corroborating the SRPAC data (Fig. 2). Hence, the presence of QS is considered for fitting the data and better fitting to the experimental data is observed with this model. This aspect is shown in Fig. 6 for the lowest temperature NFS data. Detailed fitting of the NFS data and the obtained temperature variation of QS across T_m is discussed in Sec. V.

V. DISCUSSIONS AND CONCLUSIONS

The obtained PDOS, characteristic of Sn site, from NIS measurements (Fig. 3) is shown in Fig. 7. Qualitatively, the obtained PDOS of Sn from NIS experiment across T_m is same corroborating MD simulations data (Fig. 5) indicating that there is no structural phase transition across T_m as expected. In the context of NIS measurements it is imperative to consider the vibrational modes associated only with Ti atom in the unit-cell of BTO as Sn is expected to substitute Ti atom. These modes are A_1, A_2, E^1, E^2, wherein A, E stand for vibration of Ti atom along the z axis, on the xy plane, respectively. The calculated and/or observed vibrational frequency for these modes in literature is at about 88.8 cm^{-1} (11.0 meV), 123 cm^{-1} (15.2 meV), 144 cm^{-1} (17.8 meV),

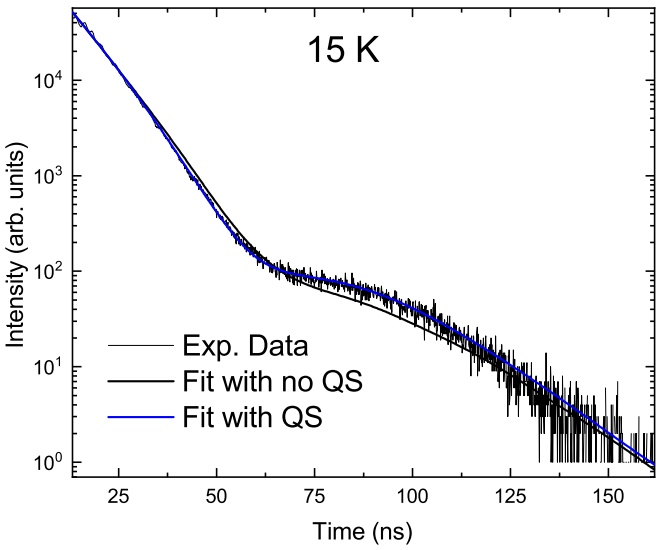

FIG. 6. Comparison of the different models to fit the low temperature NFS data. Fitting of the 15 K NFS data is shown with and without quadrupole splitting (QS).

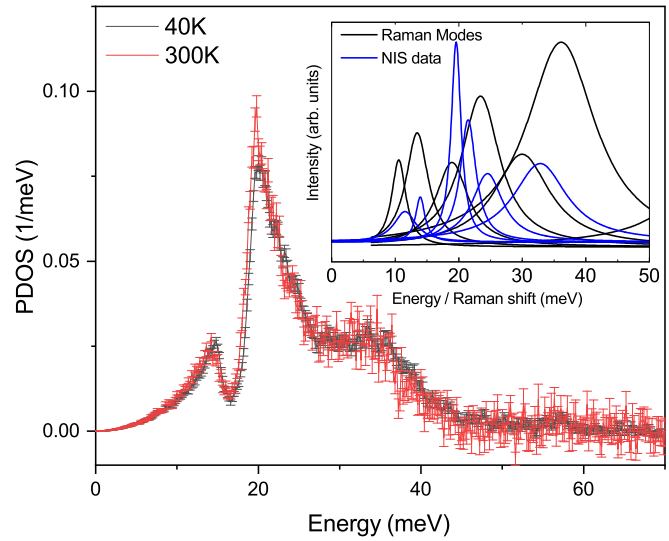

FIG. 7. Phonon density of states (PDOS) of $BaTi_{0.7}{}^{119}Sn_{0.3}O_3$ obtained from NIS measurements at 300 and 40 K. Inset shows the peaks obtained from the de-convolution of room temperature Raman [Fig. 1(d)] and NIS data.

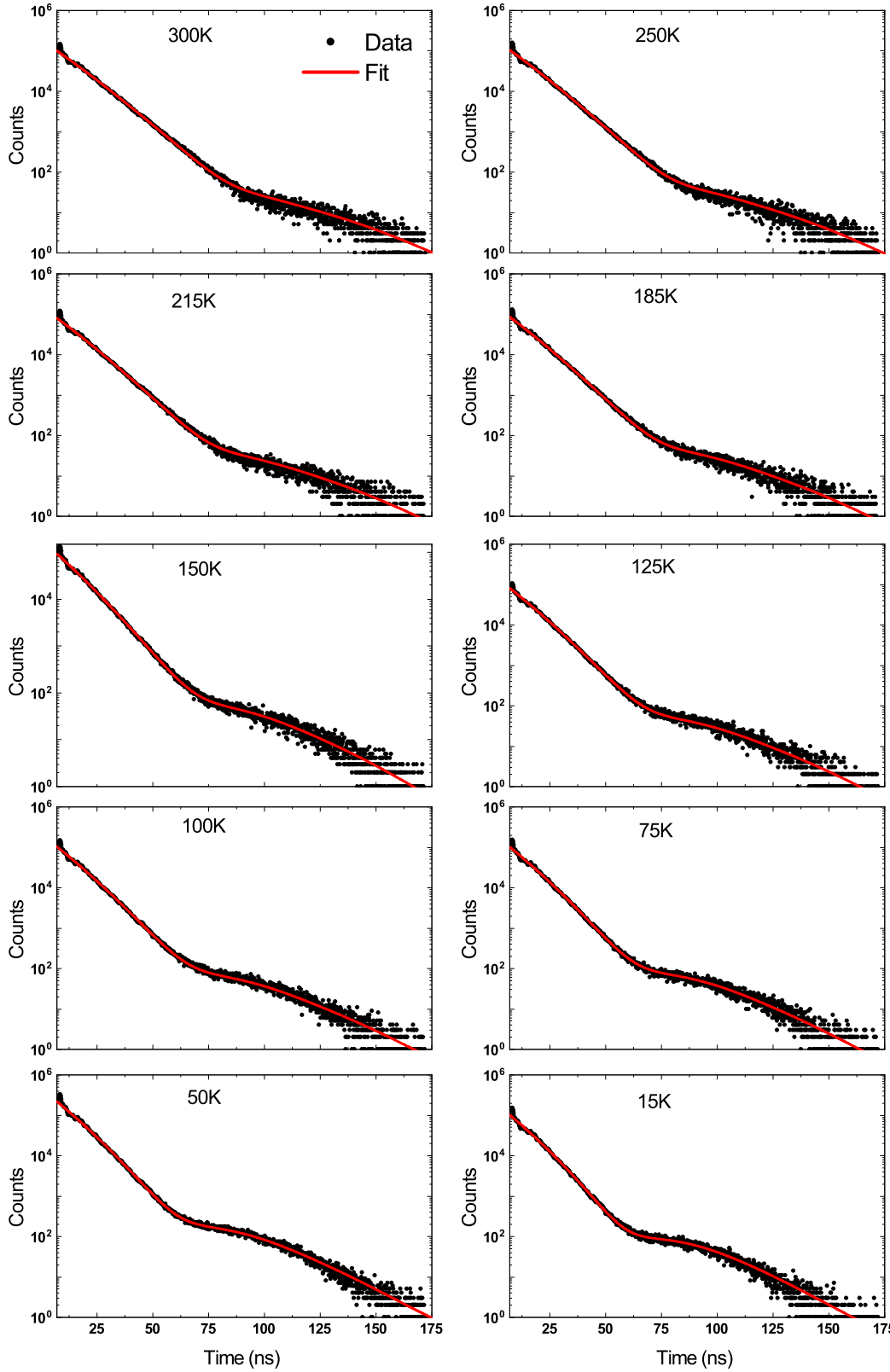

FIG. 8. Temperature dependent ^{119}Sn NFS data of $BaTi_{0.7}\,^{119}Sn_{0.3}\,O_3$. Symbols represent the experimental data points and the solid line is the best fit to the data. The obtained temperature variation of quadrupole splitting (QS) is shown in Fig. 9

170 cm^{-1} (21.2 meV), 262.7 cm^{-1} (32.6 meV), etc. [37]. The observed modes from NIS data agree with the Raman data indicating that the Sn is replacing the Ti atom in a BTO unit cell of the present study.

The experimental room temperature Raman and NIS data is deconvoluted and the obtained peaks are plotted in a single plot as shown in the inset of Fig. 7. The relative intensity of the peaks from Raman and NIS data may not be a meaningful

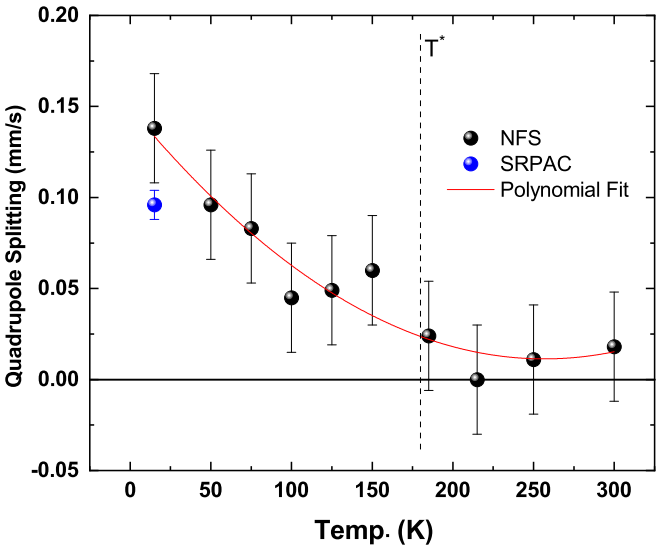

FIG. 9. Temperature dependent variation of quadrupole splitting (QS) obtained from the fitting of NFS data as shown Fig. 8. Horizontal solid line to shows the zero QS line. Vertical dashed lines are to show the T^* as obtained from the temperature dependent dielectric constant data [Fig. 1(b)]. Symbols are the experimental data points and the solid line is the second-order polynomial fit to the data. Value of QS obtained from SRPAC data (Fig. 2) is also shown.

comparison as NIS is element-specific in contrast to the collective contributions that are recorded in Raman spectroscopy measurements. However, if one sees the peak positions [inset of Fig. 7)], it is clear that the modes match reasonably well within experimental errors, although the Raman data are relatively broader.

The important observation of the present study is the development of small, but finite QS values at low temperatures in the studied relaxor as evidenced from both SRPAC (Fig. 2) and NFS (Fig. 6) measurements. The SRPAC data scaled by the exponential decay and the scaling factor, as shown in Fig. 2(b), clearly depict the long-period modulation with opposite signs in the horizontal and vertical geometry. These modulations confirm the presence of hyperfine interactions. The fit provides $\tau = 25.90 \pm 0.1$ ns which is consistent with tabulated natural decay value of 26.01 ns. The extracted QS value $\Omega = 0.096 \pm 0.008$ mm/s is similar to the value obtained in the NFS data. In view of this, and also better quality of the fit to the NFS data by considering the presence of QS (Fig. 6), all the NFS data measured at different temperatures are analyzed by keeping QS as free variable in the present work. Good quality of the fits, as shown in Fig. 8, ensures the consideration of this model as realistic one. The obtained variation of QS with temperature is shown in Fig. 9 and one can clearly see the progressive development of QS at low temperatures, below T^*. This variation is similar to that of systems with FE ordering, for example as reported in $PbTi_{1-x}Zr_xO_3$ with PAC measurements [14]. This observation corroborates roughly with the Ti K-edge x-ray absorption spectroscopy (XAS) data as reported in our earlier work [4]. The area of the feature at Ti pre-edge data was also observed to raise on lowering the temperature below T^*. These features of XAS data coming from the distortions of TiO_6 octahedron are shown to originate from the off-center Ti displacement within the TiO_6 octahedra, raising the electric dipole moment with decreasing temperature.

Further, in the present work the QS is observed to vary with temperature in a different fashion as compared to conventional FE materials. Especially in BTO it is reported that the QS/EFG, square of polarization (P_S^2), tetragonal strain etc., follow the same trend with temperature. i.e., an almost constant saturated value and a sudden vanishing value close to Curie temperature (T_C) [9,10]. However, the temperature variation of QS in the present work is well fitted with a polynomial of second order $QS(\text{mm/s}) = A + BT + CT^2$ with the parameters A as $0.149 \pm 0.013\,\text{mm.s}^{-1}$; B as $1.1 \times 10^{-3} \pm 1.9 \times 10^{-4}\,\text{mm.s}^{-1}.\text{K}^{-1}$ and C as $2.1 \times 10^{-6} \pm 5.8 \times 10^{-7}\,\text{mms}^{-1}\text{K}^{-2}$. One of the reasons for this could be due to the contribution from dynamic EFG at low temperatures in relaxors as compared to robust FE materials. As the temperature is lowered more and more PNRs freeze and grow in size, therefore, the relaxation rate of polarization and hence EFG falls within the time domain of Mössbauer spectroscopy.

In conclusion, the present work has unambiguously demonstrated the signatures of ferroelectriclike distortions, specifically the presence of EFG at the Ti/Sn site in isovalent (Sn^{4+}) substituted $BaTiO_3$ based relaxor systems. The obtained results can be attributed to the distortion in the cubic structure caused by the Sn substitution at Ti sites in BTO. These findings were achieved through the combined use of synchrotron-based hyperfine interaction techniques, vibrational spectroscopy, and molecular dynamic simulations. This study highlights the importance of employing experimental methods that can offer complementary insights into the atomic-scale structural distortions resulting in EFG, thereby contributing to a more reliable understanding of relaxor-type materials.

ACKNOWLEDGMENTS

V.R.R. acknowledges the financial support by the Department of Science and Technology, New Delhi provided within the framework of the India@DESY collaboration for NFS measurements at P-01, PETRA-III. We are grateful for the help of R. Raj during NFS measurements. M.D. thank Department of Science and Technology, New Delhi for the fellowship in the form of DST INSPIRE (IF200026). V.R.R. acknowledges funding from DST-SERB-CRG/2022/001805. C.M. acknowledges funding from SERB (Ramanujan Fellowship, File No. RJF/2021/00012). G.B. thank University Grants Commission, New Delhi for the Dr. D.S. Kothari Post-Doctoral Fellowship (Grant No. F.4-2/2006 (BSR)/PH/20-21/0166). Dr. Sathe is thanked for Raman data.

[1] G. Burns and F. H. Dacol, Crystalline ferroelectrics with glassy polarization behavior, Phys. Rev. B **28**, 2527 (1983).

[2] R. López-Juárez, F. González, and M.-E. Villafuerte-Castrejón, Lead-free ferroelectric ceramics with perovskite structure, in

Ferroelectrics-Material Aspects, edited by M. Lallart (Intech, Rijeka, Croatia, 2011).

[3] S. K. Upadhyay, V. R. Reddy, P. Bag, R. Rawat, S. Gupta, and A. Gupta, Electro-caloric effect in lead-free Sn doped $BaTiO_3$ ceramics at room temperature and low applied fields, Appl. Phys. Lett. **105**, 112907 (2014).

[4] A. Surampalli, I. Schiesaro, P. Corsi, C. Meneghini, V. G. Sathe, A. Sagdeo, A. K. Sinha, G. Aquilanti, E. Welter, and V. R. Reddy, Evidence of structural modifications in the region around the broad dielectric maxima in the 30% Sn-doped barium titanate relaxor, Phys. Rev. B **100**, 134104 (2019).

[5] A. Surampalli, R. Egli, D. Prajapat, C. Meneghini, and V. R. Reddy, Reentrant phenomenon in the diffuse ferroelectric $BaSn_{0.15}Ti_{0.85}O_3$:Local structural insights and first-order reversal curves study, Phys. Rev. B **104**, 184114 (2021).

[6] C. Mentzer, S. Lisenkov, Z. G. Fthenakis, and I. Ponomareva, Phase evolution in the ferroelectric relaxor $Ba(Ti_{1-x}, Zr_x)O_3$ from atomistic simulations, Phys. Rev. B **99**, 064111 (2019).

[7] V. Westphal, W. Kleemann, and M. D. Glinchuk, Diffuse phase transitions and random-field-induced domain states of the "relaxor"ferroelectric $PbMg_{1/3}Nb_{2/3}O_3$, Phys. Rev. Lett. **68**, 847 (1992).

[8] W. Kleemann, Random fields in relaxor ferroelectrics—a jubilee review, J. Adv. Dielectr. **02**, 1241001 (2012).

[9] V. Bhide and M. Multani, Mössbauer effect for Fe^{57} in ferroelectric $BaTiO_3$. II. the vacancy-impurity associated state, Phys. Rev. **149**, 289 (1966).

[10] V. Bhide and V. Durge, Sn^{119} Mössbauer studies of lower transitions in barium titanate, Solid State Commun. **10**, 401 (1972).

[11] A. Jain, S. Shringi, and M. Sharma, Temperature-dependent optical mode in antiferroelectric $PbZrO_3$ by the Mössbauer effect, Phys. Rev. B **2**, 2756 (1970).

[12] E. Stern, Character of order-disorder and displacive components in barium titanate, Phys. Rev. Lett. **93**, 037601 (2004).

[13] G. L. Catchen, S. J. Wukitch, D. M. Spaar, and M. Blaszkiewicz, Temperature dependence of the nuclear quadrupole interactions at Ti sites in ferroelectric $PbTiO_3$ and in ilmenite and perovskite $CdTiO_3$: Evidence for order-disorder phenomena, Phys. Rev. B **42**, 1885 (1990).

[14] R. Alonso, A. L. García, A. Ayala, and P. De la Presa, Temperature dependence of the nuclear quadrupole interaction at Zr-Ti sites in in the Zr-rich rhombohedral and cubic phases, J. Phys.: Condens. Matter **10**, 2139 (1998).

[15] J. N. Gonçalves, A. Stroppa, J. G. Correia, T. Butz, S. Picozzi, A. S. Fenta, and V. S. Amaral, *Ab initio* study of the relation between electric polarization and electric field gradients in ferroelectrics, Phys. Rev. B **86**, 035145 (2012).

[16] V. Veerapandiyan, M. N. Popov, F. Mayer, J. Spitaler, S. Svirskas, V. Kalendra, J. Lins, G. Canu, M. T. Buscaglia, M. Pasciak *et al.*, Origin of relaxor behavior in barium-titanate-based lead-free perovskites, Adv. Electron. Mater. **8**, 2100812 (2022).

[17] I. Sergueev, U. van Bürck, A. I. Chumakov, T. Asthalter, G. V. Smirnov, H. Franz, R. Rüffer, and W. Petry, Synchrotron-radiation-based perturbed angular correlations used in the investigation of rotational dynamics in soft matter, Phys. Rev. B **73**, 024203 (2006).

[18] I. Sergueev, O. Leupold, H.-C. Wille, T. Roth, A. I. Chumakov, and R. Rüffer, Hyperfine interactions in ^{61}Ni with synchrotron-radiation-based perturbed angular correlations, Phys. Rev. B **78**, 214436 (2008).

[19] C. Strohm, I. Sergueev, and U. van Bürck, Synchrotron-radiation–based perturbed angular correlations from ^{119}Sn, Europhys. Lett. **81**, 52001 (2008).

[20] D. Bessas, I. Sergueev, K. Glazyrin, C. Strohm, I. Kupenko, D. G. Merkel, G. J. Long, F. Grandjean, A. I. Chumakov, and R. Rüffer, Revealing the hidden hyperfine interactions in ε-iron, Phys. Rev. B **101**, 035112 (2020).

[21] A. Chumakov and R. Rüffer, Nuclear inelastic scattering, Hyperfine Interact. **113**, 59 (1998).

[22] L. Bocklage, NEXUS - Nuclear elastic x-ray scattering universal software, FS-photon science (2023), https://helmholtz.software/software/nuclear-nexus.

[23] S. Plimpton, Fast parallel algorithms for short-range molecular dynamics, J. Comput. Phys. **117**, 1 (1995).

[24] P. Ewald, Die berechnung optischer und elektrostatischer gitterpotentiale, Ann. Phys. **369**, 253 (2006).

[25] A. Pedone, G. Malavasi, M. C. Menziani, A. N. Cormack, and U. Segre, A new self-consistent empirical interatomic potential model for oxides, silicates, and silica-based glasses, J. Phys. Chem. B **110**, 11780 (2006).

[26] B. W. H. van Beest, G. J. Kramer, and R. A. van Santen, Force fields for silicas and aluminophosphates based on *ab initio* calculations, Phys. Rev. Lett. **64**, 1955 (1990).

[27] S. Nose, A unified formulation of the constant temperature molecular dynamics methods, J. Chem. Phys. **81**, 511 (1984).

[28] W. G. Hoover, Canonical dynamics: Equilibrium phase-space distributions, Phys. Rev. A **31**, 1695 (1985).

[29] W. Shinoda, M. Shiga, and M. Mikami, Rapid estimation of elastic constants by molecular dynamics simulation under constant stress, Phys. Rev. B **69**, 134103 (2004).

[30] G. J. Martyna, D. J. Tobias, and M. L. Klein, Constant pressure molecular dynamics algorithms, J. Chem. Phys. **101**, 4177 (1994).

[31] J. Rodríguez-Carvajal, Recent advances in magnetic structure determination by neutron powder diffraction, Phys. B **192**, 55 (1993).

[32] A. Kumar, I. Rivera, and R. Katiyar, Investigation of local structure of lead-free relaxor $Ba(Ti_{0.70}Sn_{0.30})O_3$ by Raman spectroscopy, J. Raman Spectrosc. **40**, 459 (2009).

[33] C. Lei, A. A. Bokov, and Z.-G. Ye, Ferroelectric to relaxor crossover and dielectric phase diagram in the $BaTiO_3 - BaSnO_3$ system, J. Appl. Phys. **101**, 084105 (2007).

[34] U. D. Venkateswaran, V. M. Naik, and R. Naik, High-pressure Raman studies of polycrystalline $BaTiO_3$, Phys. Rev. B **58**, 14256 (1998).

[35] R. Naik, J. J. Nazarko, C. S. Flattery, U. D. Venkateswaran, V. M. Naik, M. S. Mohammed, G. W. Auner, J. V. Mantese, N. W. Schubring, A. L. Micheli *et al.*, Temperature dependence of the Raman spectra of polycrystalline $Ba_{1-x}Si_xTiO_3$, Phys. Rev. B **61**, 11367 (2000).

[36] S. Sanna, C. Thierfelder, S. Wippermann, T. P. Sinha, and W. G. Schmidt, Barium titanate ground-and excited-state properties from first-principles calculations, Phys. Rev. B **83**, 054112 (2011).

[37] W. An, T.-H. Liu, C.-H. Wang, C.-L. Diao, N.-N. Luo, Y. Liu, Z.-M. Qi, T. Shao, Y.-Y. Wang, H. Jiao *et al.*, Assignment for vibrational spectra of $BaTiO_3$ ferroelectric ceramic based on the first principles calculation, Acta Phys. **31**, 1059 (2015).

[38] H.-Y. Zhang, Z.-Y. Zeng, Y.-Q. Zhao, Q. Lu, and Y. Cheng, First-principles study of lattice dynamics, structural phase transition, and thermodynamic properties of barium titanate, Z. Naturforsch. A **71**, 759 (2016).

[39] Y.-S. Seo and J. S. Ahn, Pressure dependence of the phonon spectrum in $BaTiO_3$ polytypes studied by *ab initio* calculations, Phys. Rev. B **88**, 014114 (2013).

[40] A. Mahmoud, A. Erba, K. E. El-Kelany, M. Rérat, and R. Orlando, Low-temperature phase of $BaTiO_3$: Piezoelectric, dielectric, elastic, and photoelastic properties from ab initio simulations, Phys. Rev. B **89**, 045103 (2014).

[41] W. Preis, Molecular dynamics simulations of oxygen diffusion in barium titanate doped with Mg and Ca, J. Solid State Chem. **312**, 123290 (2022).

[42] L. Zhou, X.-L. Zhang, Y.-Y. Cao, F. Zheng, H. Gao, H.-F. Liu, and Z. Ma, Prediction of flexoelectricity in $BaTiO_3$ using molecular dynamics simulations, Chin. Phys. B **32**, 017701 (2023).